

Electronic Supplementary Information (ESI)

A wheel-like polyoxometalate for haloperoxidase inspired antibiofouling with H₂O₂ *in-situ* provided by electrocatalysis

Yumeng Bian,^{#a} Runze Wang, ^{#a} Xinxin Xu, ^{*a} Jin Chen ^b and Qiang Wang ^{*b}

^a Department of Chemistry, College of Science, Northeastern University, Shenyang 110819, Liaoning, China

^b Key Laboratory of Electromagnetic Processing of Materials, Ministry of Education, Northeastern University, Shenyang 110819, Liaoning, China

Materials and characterization

All chemicals were of analytical grade, commercially available from Sinopharm Chemical Reagent Co. Ltd (Shanghai, China) and used as received without further purification. XPS was performed on photoelectron spectroscopy (ESCALAB 250Xi, Thermo Fisher Scientific). UV-Vis spectrometer (T6 new century, Persee) was used to study haloperoxidase mimic activity. Electrochemical tests were conducted on electrochemical workstation (CHI-760E, Chenhua).

Single-crystal X-ray diffraction

Single crystal of **Ni₁₆Mo₁₆P₂₄** was selected under an optical microscope and glued on a glass fiber. Structural measurement was performed with a Bruker AXS SMART APEX II CCD diffractometer at 293 K. The structure was solved with direct methods and refined by using the full-matrix least-squares method on F² with the Olex2 software (Table S1 and S2). Anisotropic thermal parameters were used to refine all non-hydrogen atoms. Carbon-bound hydrogen atoms were placed in geometrically calculated positions. CIF file (CCDC 2315001) contains supplementary crystallographic data for this paper. The file can be obtained free of charge via www.ccdc.cam.ac.uk/data_request/cif (Cambridge Crystallographic Data Centre).

Haloperoxidase mimic activity

Haloperoxidase mimic activity was determined by bromination of PR with Br⁻ and H₂O₂. UV-visible spectrometer (UV-Vis) was employed to measure the solution containing PR, NH₄Br, H₂O₂ and **Ni₁₆Mo₁₆P₂₄**. Reaction velocity was studied with time course mode by monitoring the absorbance at 590 nm based on [Br₄PR]. Lambert-Beer law is employed to calculate [Br₄PR] and the extinction coefficient of Br₄PR (ϵ -Br₄PR) was 72200 M⁻¹·cm⁻¹. In kinetic tests, concentration of one reactant changed while

others kept constant. Test was carried out until slope became constant to calculate kinetic parameters. All the tests were conducted for three times and the variations were exhibited with error bars.

RDE and RRDE tests

RDE test was conducted in O₂ saturated PBS (0.1 M, pH = 7.4) with three-electrode system, in which carbon rod and saturated calomel electrode were employed as counter and reference electrodes. Working electrode was fabricated as follows: the mixture of **Ni₁₆Mo₁₆P₂₄** (2 mg) and carbon black (Vulcan XC-72R, 8 mg) was dispersed in aqueous solution of water (0.8 mL), ethanol (0.15 mL) and 50 µL Nafion (5 %). The ink (10 µL) was dropped on RDE (electrode area is 0.196 cm²) and served as working electrode. Linear sweep voltammetry (LSV) was recorded at 10 mV·s⁻¹. The rotating speed of RDE was 400, 625, 900, 1225 and 1600 rpm. The electron transfer number was calculated by the Koutechy-Levich (K-L) equation (Eq. 1). In this equation, j is the measured current density, j_k is the kinetic current density, ω is the electrode rotating rate. The parameter B can be calculated from the slope of the K-L plots based on the following Levich equation (Eq. 2), in which n is the electron transfer number per oxygen molecule, F is the Faraday constant, D₀ is the diffusion coefficient of O₂, ν is the kinetic viscosity and C₀ is the bulk concentration of O₂.

$$1/j = 1/j_k + 1/B\omega^{1/2} \quad (1)$$

$$B = 0.62nF(D_0)^{2/3}(V)^{-1/6}C_0 \quad (2)$$

RRDE experiment was also conducted in O₂ saturated PBS (0.1 M, pH = 7.4). Working electrode was fabricated as follows: the mixture of **Ni₁₆Mo₁₆P₂₄** (2 mg) and carbon black (Vulcan XC-72R, 8 mg) was dispersed in aqueous solution of water (0.8 mL), ethanol (0.15 mL) and 50 µL Nafion (5 %). The ink (10 µL) was dropped on RRDE and

served as working electrode. Carbon rod and saturated calomel electrode were employed as counter and reference electrodes. The disk potential was cycled from 0 to 1.0 V (vs. RHE) with a scan rate of $10 \text{ mV}\cdot\text{s}^{-1}$. The ring potential was constant at 1.2 V (vs. RHE). The H_2O_2 selectivity and electron transfer number (n) were calculated with Eq. 3 and 4. In these equations, I_D and I_R represent the disk and ring currents density. N ($N = 0.37$, obtained from $\text{K}_3\text{Fe}(\text{CN})_6$ reduction experiments at various rotation rates) is the current collection efficiency of the Pt ring.

$$\text{H}_2\text{O}_2 \% = (200 \times I_R/N) / (I_R/N + I_D) \quad (3)$$

$$n = 4 \times I_d / (I_R/N + I_D) \quad (4)$$

H₂O₂ production performance

The H_2O_2 production test was studied in an H-cell device at room temperature. During test, the electrolyte (PBS, 0.1 M, pH = 7.4) was continuously purged with O_2 . A constant electrolytic voltage of 0.1, 0.3 and 0.5 V (vs. RHE) was applied for H_2O_2 production. Aliquots in the cathode room was take collected every 20 min and titrated against $\text{Ce}(\text{SO}_4)_2$. The concentration of H_2O_2 evolved increased linearly with time, which indicates $\text{Ni}_{16}\text{Mo}_{16}\text{P}_{24}$ had good stability.

Computational method

All the density functional theory (DFT) calculations were performed by Vienna Ab-initio Simulation Package (VASP), employing the Projected Augmented Wave (PAW) method. The revised Perdew-Burke-Ernzerhof (RPBE) functional was used to describe the exchange and correlation effects. For all the geometry optimizations, the cutoff energy was set to be 400 eV. A $3 \times 3 \times 1$ Monkhorst-Pack grid was used to carry out the surface calculations on the surface of $\text{Ni}_{16}\text{Mo}_{16}\text{P}_{24}$. Free energy of an adsorbed species is defined as $\Delta G_{\text{ads}} = \Delta E_{\text{ads}} + \Delta E_{\text{ZPE}} - T\Delta S_{\text{ads}}$, in which ΔE_{ads} is the electronic

adsorption energy, ΔE_{ZPE} is the zero point energy difference between adsorbed and gaseous species, and $T\Delta S_{ads}$ is the corresponding entropy difference between these two states.

Antibiofouling experiment

E. coli was incubated at 37 °C for 12 h. The bacteria was separated from medium by centrifugation at 5000 rpm for 5 min. Bacteria was then diluted and suspended in 0.1 M PBS. PBS mediums containing 10^7 cfu·mL⁻¹ *E. coli* were prepared for antibiofouling experiments. *E. coli* (10 mL, 10^7 cfu·mL⁻¹) was oscillated cultivation with Ti plate coated by **Ni₁₆Mo₁₆P₂₄** for 2 h at 37 °C. In this test, the concentration of NH₄Br was 0.4 mM. After that, surface of Ti plate coated by **Ni₁₆Mo₁₆P₂₄** was gently washed by sterile PBS. Subsequently, Ti plate coated by **Ni₁₆Mo₁₆P₂₄** was dyed with 4', 6-diamidino-2-phenylindole (DAPI, 1 µg·mL⁻¹). Observation was performed by fluorescence microscopy. Antibiofouling tests for *S. aures* were conducted in same way. For antibiofouling with H₂O₂ in-situ provided by ORR, three-electrode system was used. Carbon rod and saturated calomel electrode were employed as counter and reference electrodes. Working electrode and **Ni₁₆Mo₁₆P₂₄** ink was fabricated as above RDE test. Ti plate was used as current collector for working electrode. Before antibiofouling, the H₂O₂ production test was conducted for 30 min at 0.3 V (vs. RHE).

Table S1. Crystal data and structure refinement for **Ni₁₆Mo₁₆P₂₄**.

Empirical formula	C ₁₀ H ₈ Mo ₈ N ₃ Ni ₉ O ₈₆ P ₁₃
Formula weight	3244.71
Crystal system	Triclinic
Space group	P-1
a (Å)	15.5877(2)
b (Å)	17.2833(3)
c (Å)	18.8306(3)
α (°)	67.3750(10)
β (°)	71.7960(10)
γ (°)	81.9550(10)
Volume (Å ³)	4447.18(12)
Z	2
F(000)	3120
Reflections collected/unique	87234/29959
R(int)	0.0291
Goodness of fit on F ²	1.132
R ₁	0.0478
wR ₂	0.1806

Table S2. Selected bond lengths (Å) and angles (°) of **Ni₁₆Mo₁₆P₂₄**

Mo(1)-O(69)	1.680(4)	Mo(2)-O(57)	1.671(4)
Mo(1)-O(26)	1.935(3)	Mo(2)-O(34)	1.960(3)
Mo(1)-O(9)	1.944(3)	Mo(2)-O(33)	1.973(3)
Mo(1)-O(29)#1	2.008(3)	Mo(2)-O(25)	2.071(3)
Mo(1)-O(50)	2.071(4)	Mo(2)-O(36)#1	2.077(3)
Mo(1)-O(5)	2.473(3)	Mo(2)-O(13)	2.211(4)
Mo(3)-O(35)	1.675(4)	Mo(4)-O(49)	1.691(4)
Mo(3)-O(3)	1.944(3)	Mo(4)-O(26)	1.951(3)
Mo(3)-O(21)	1.956(3)	Mo(4)-O(9)	1.957(3)
Mo(3)-O(43)#1	2.073(3)	Mo(4)-O(2)	2.058(3)
Mo(3)-O(23)	2.079(3)	Mo(4)-O(15)#1	2.089(3)
Mo(3)-O(5)	2.383(3)	Mo(4)-O(39)	2.186(3)
Mo(5)-O(53)	1.684(4)	Mo(6)-O(64)	1.675(4)
Mo(5)-O(3)	1.950(3)	Mo(6)-O(12)	1.936(3)
Mo(5)-O(21)	1.966(3)	Mo(6)-O(7)	1.929(3)
Mo(5)-O(19)	2.069(3)	Mo(6)-O(27)	2.064(4)
Mo(5)-O(8)	2.074(4)	Mo(6)-O(58)	2.074(3)
Mo(5)-O(31)	2.184(3)	Mo(6)-O(14)	2.386(3)
Mo(7)-O(40)	1.678(4)	Mo(8)-O(52)	1.679(4)
Mo(7)-O(34)	1.933(3)	Mo(8)-O(7)	1.956(3)
Mo(7)-O(33)	1.944(3)	Mo(8)-O(12)	1.984(3)
Mo(7)-O(18)	2.041(3)	Mo(8)-O(17)	2.069(3)
Mo(7)-O(37)	2.054(4)	Mo(8)-O(22)	2.080(3)
Mo(7)-O(14)	2.469(4)	Mo(8)-O(38)	2.189(3)
Ni(8)-O(6)	2.033(4)	Ni(9)-O(21)	2.015(3)
Ni(8)-O(6)#2	2.033(4)	Ni(9)-O(68)	2.076(5)
Ni(8)-O(4)	2.092(3)	Ni(9)-O(44)	2.083(3)
Ni(8)-O(4)#2	2.092(3)	Ni(9)-O(24)	2.131(3)
Ni(8)-O(30)	2.324(4)	Ni(9)-O(11)	2.176(3)
Ni(8)-O(30)#2	2.324(4)	Ni(9)-O(51)	2.267(4)
Ni(7)-O(34)	2.047(3)	Ni(6)-O(3)#1	2.021(3)
Ni(7)-O(78)	2.072(4)	Ni(6)-O(74)	2.079(4)
Ni(7)-O(60)	2.076(3)	Ni(6)-O(20)	2.083(3)
Ni(7)-O(28)	2.082(4)	Ni(6)-O(48)	2.089(3)
Ni(7)-O(61)	2.104(3)	Ni(6)-O(55)#1	2.106(4)
Ni(7)-O(32)	2.217(4)	Ni(6)-O(54)	2.220(4)
Ni(5)-O(20)	2.032(3)	Ni(4)-O(9)	2.038(3)
Ni(5)-O(26)#1	2.041(3)	Ni(4)-O(70)	2.062(4)
Ni(5)-O(16)	2.072(3)	Ni(4)-O(61)	2.099(3)
Ni(5)-O(30)	2.077(3)	Ni(4)-O(60)	2.116(4)
Ni(5)-O(46)	2.109(3)	Ni(4)-O(11)	2.183(3)
Ni(5)-O(54)	2.323(4)	Ni(4)-O(51)	2.210(4)
Ni(10)-O(81)#1	2.114(11)	Ni(3)-O(12)	1.997(3)

Ni(10)-O(81)	2.114(11)	Ni(3)-O(46)	2.041(3)
Ni(10)-O(79)#1	2.066(5)	Ni(3)-O(16)	2.123(3)
Ni(10)-O(79)	2.066(5)	Ni(3)-O(56)	2.126(4)
Ni(10)-O(80)#1	2.105(7)	Ni(3)-O(42)	2.196(4)
Ni(10)-O(80)	2.105(7)	Ni(3)-O(10)	2.211(3)
Ni(2)-O(33)	2.030(3)	Ni(1)-O(7)	2.029(3)
Ni(2)-O(71)	2.078(4)	Ni(1)-O(24)	2.050(3)
Ni(2)-O(48)	2.088(4)	Ni(1)-O(73)	2.056(5)
Ni(2)-O(55)#1	2.104(4)	Ni(1)-O(28)	2.066(4)
Ni(2)-O(42)	2.200(4)	Ni(1)-O(44)	2.077(3)
Ni(2)-O(10)	2.202(3)	Ni(1)-O(32)	2.361(4)
O(69)-Mo(1)-O(26)	104.37(17)	O(57)-Mo(2)-O(34)	102.10(18)
O(69)-Mo(1)-O(9)	102.51(17)	O(57)-Mo(2)-O(33)	102.71(17)
O(26)-Mo(1)-O(9)	94.73(13)	O(34)-Mo(2)-O(33)	93.57(14)
O(69)-Mo(1)-O(29)#1	97.30(17)	O(57)-Mo(2)-O(25)	96.46(18)
O(26)-Mo(1)-O(29)#1	87.90(14)	O(34)-Mo(2)-O(25)	86.42(14)
O(9)-Mo(1)-O(29)#1	158.67(15)	O(33)-Mo(2)-O(25)	160.37(16)
O(69)-Mo(1)-O(50)	95.66(18)	O(57)-Mo(2)-O(36)#1	94.36(18)
O(26)-Mo(1)-O(50)	159.09(15)	O(34)-Mo(2)-O(36)#1	162.60(15)
O(9)-Mo(1)-O(50)	86.62(14)	O(33)-Mo(2)-O(36)#1	88.23(13)
O(29)#1-Mo(1)-O(50)	83.60(15)	O(25)-Mo(2)-O(36)#1	86.15(14)
O(69)-Mo(1)-O(5)	173.18(16)	O(57)-Mo(2)-O(13)	173.31(16)
O(26)-Mo(1)-O(5)	81.79(13)	O(34)-Mo(2)-O(13)	83.09(14)
O(9)-Mo(1)-O(5)	79.61(12)	O(33)-Mo(2)-O(13)	81.00(13)
O(29)#1-Mo(1)-O(5)	79.83(12)	O(25)-Mo(2)-O(13)	79.52(15)
O(50)-Mo(1)-O(5)	77.93(13)	O(36)#1-Mo(2)-O(13)	80.10(14)
O(35)-Mo(3)-O(3)	105.43(17)	O(49)-Mo(4)-O(26)	103.55(17)

O(35)-Mo(3)-O(21)	102.22(17)	O(49)-Mo(4)-O(9)	103.58(17)
O(3)-Mo(3)-O(21)	94.44(13)	O(26)-Mo(4)-O(9)	93.78(13)
O(35)-Mo(3)-	92.00(17)	O(49)-Mo(4)-O(2)	93.51(17)
O(43)#1			
O(3)-Mo(3)-O(43)#1	86.81(14)	O(26)-Mo(4)-O(2)	161.52(15)
O(21)-Mo(3)-	164.80(14)	O(9)-Mo(4)-O(2)	89.02(13)
O(43)#1			
O(35)-Mo(3)-O(23)	92.59(17)	O(49)-Mo(4)-	94.76(17)
		O(15)#1	
O(3)-Mo(3)-O(23)	160.68(15)	O(26)-Mo(4)-	87.92(13)
		O(15)#1	
O(21)-Mo(3)-O(23)	88.35(14)	O(9)-Mo(4)-	160.60(14)
		O(15)#1	
O(43)#1-Mo(3)-	85.64(15)	O(2)-Mo(4)-	83.55(13)
O(23)		O(15)#1	
O(35)-Mo(3)-O(5)	170.69(16)	O(49)-Mo(4)-	171.27(16)
		O(39)	
O(3)-Mo(3)-O(5)	83.38(13)	O(26)-Mo(4)-	83.00(13)
		O(39)	
O(21)-Mo(3)-O(5)	79.74(12)	O(9)-Mo(4)-O(39)	81.48(13)
O(43)#1-Mo(3)-O(5)	85.37(13)	O(2)-Mo(4)-O(39)	79.35(14)
O(23)-Mo(3)-O(5)	78.31(13)	O(15)#1-Mo(4)-	79.55(13)
		O(39)	
O(53)-Mo(5)-O(3)	102.83(16)	O(64)-Mo(6)-	102.36(18)
		O(12)	
O(53)-Mo(5)-O(21)	102.35(16)	O(64)-Mo(6)-O(7)	104.38(17)
O(3)-Mo(5)-O(21)	93.94(14)	O(12)-Mo(6)-O(7)	95.29(14)
O(53)-Mo(5)-O(19)	93.47(18)	O(64)-Mo(6)-	93.01(17)
		O(27)	
O(3)-Mo(5)-O(19)	161.84(16)	O(12)-Mo(6)-	163.61(15)
		O(27)	
O(21)-Mo(5)-O(19)	90.29(14)	O(7)-Mo(6)-O(27)	86.22(14)
O(53)-Mo(5)-O(8)	97.73(17)	O(64)-Mo(6)-	93.48(17)
		O(58)	
O(3)-Mo(5)-O(8)	86.57(14)	O(12)-Mo(6)-	87.88(14)
		O(58)	
O(21)-Mo(5)-O(8)	159.25(15)	O(7)-Mo(6)-O(58)	160.68(15)
O(19)-Mo(5)-O(8)	83.31(14)	O(27)-Mo(6)-	85.53(15)
		O(58)	
O(53)-Mo(5)-O(31)	171.86(16)	O(64)-Mo(6)-	171.76(16)
		O(14)	
O(3)-Mo(5)-O(31)	84.48(14)	O(12)-Mo(6)-	80.61(13)
		O(14)	
O(21)-Mo(5)-O(31)	80.46(13)	O(7)-Mo(6)-O(14)	82.84(13)

O(19)-Mo(5)-O(31)	78.81(15)	O(27)-Mo(6)-O(14)	83.40(13)
O(8)-Mo(5)-O(31)	78.95(14)	O(58)-Mo(6)-O(14)	78.87(13)
O(40)-Mo(7)-O(34)	103.75(17)	O(52)-Mo(8)-O(7)	102.69(17)
O(40)-Mo(7)-O(33)	102.92(17)	O(52)-Mo(8)-O(12)	102.60(17)
O(34)-Mo(7)-O(33)	95.36(14)	O(7)-Mo(8)-O(12)	92.95(14)
O(40)-Mo(7)-O(18)	94.98(17)	O(52)-Mo(8)-O(17)	96.46(18)
O(34)-Mo(7)-O(18)	159.87(15)	O(7)-Mo(8)-O(17)	86.62(13)
O(33)-Mo(7)-O(18)	87.47(14)	O(12)-Mo(8)-O(17)	160.53(15)
O(40)-Mo(7)-O(37)	94.09(17)	O(52)-Mo(8)-O(22)	92.74(18)
O(34)-Mo(7)-O(37)	87.27(14)	O(7)-Mo(8)-O(22)	163.50(15)
O(33)-Mo(7)-O(37)	161.59(15)	O(12)-Mo(8)-O(22)	89.32(14)
O(18)-Mo(7)-O(37)	84.05(15)	O(17)-Mo(8)-O(22)	85.84(14)
O(40)-Mo(7)-O(14)	171.59(15)	O(52)-Mo(8)-O(38)	173.27(16)
O(34)-Mo(7)-O(14)	84.01(13)	O(7)-Mo(8)-O(38)	83.30(14)
O(33)-Mo(7)-O(14)	79.24(13)	O(12)-Mo(8)-O(38)	79.93(13)
O(18)-Mo(7)-O(14)	76.93(13)	O(17)-Mo(8)-O(38)	80.69(14)
O(37)-Mo(7)-O(14)	82.93(13)	O(22)-Mo(8)-O(38)	81.00(15)
O(21)-Ni(9)-O(68)	86.08(16)	O(6)-Ni(8)-O(6)#2	180.00(15)
O(21)-Ni(9)-O(44)	166.39(14)	O(6)-Ni(8)-O(4)	88.76(14)
O(68)-Ni(9)-O(44)	84.73(16)	O(6)#2-Ni(8)-O(4)	91.24(14)
O(21)-Ni(9)-O(24)	93.91(13)	O(6)-Ni(8)-O(4)#2	91.24(14)
O(68)-Ni(9)-O(24)	98.98(19)	O(6)#2-Ni(8)-O(4)#2	88.76(14)
O(44)-Ni(9)-O(24)	77.67(13)	O(4)-Ni(8)-O(4)#2	180.0(3)
O(21)-Ni(9)-O(11)	88.53(13)	O(6)-Ni(8)-O(30)	95.13(13)
O(68)-Ni(9)-O(11)	168.45(17)	O(6)#2-Ni(8)-O(30)	84.87(13)
O(44)-Ni(9)-O(11)	102.23(13)	O(4)-Ni(8)-O(30)	96.47(12)
O(24)-Ni(9)-O(11)	91.57(14)	O(4)#2-Ni(8)-O(30)	83.53(12)
O(21)-Ni(9)-O(51)	101.21(13)	O(6)-Ni(8)-O(30)#2	84.87(13)

O(68)-Ni(9)-O(51)	97.72(18)	O(6)#2-Ni(8)-O(30)#2	95.13(13)
O(44)-Ni(9)-O(51)	89.97(13)	O(4)-Ni(8)-O(30)#2	83.53(12)
O(24)-Ni(9)-O(51)	158.15(14)	O(4)#2-Ni(8)-O(30)#2	96.47(12)
O(11)-Ni(9)-O(51)	73.32(13)	O(30)-Ni(8)-O(30)#2	180.00(14)
O(34)-Ni(7)-O(78)	88.20(16)	O(3)#1-Ni(6)-O(74)	88.22(16)
O(34)-Ni(7)-O(60)	98.54(14)	O(3)#1-Ni(6)-O(20)	91.81(13)
O(78)-Ni(7)-O(60)	103.01(19)	O(74)-Ni(6)-O(20)	105.35(17)
O(34)-Ni(7)-O(28)	91.62(14)	O(3)#1-Ni(6)-O(48)	172.15(15)
O(78)-Ni(7)-O(28)	100.66(18)	O(74)-Ni(6)-O(48)	84.80(16)
O(60)-Ni(7)-O(28)	154.46(15)	O(20)-Ni(6)-O(48)	93.49(14)
O(34)-Ni(7)-O(61)	171.94(15)	O(3)#1-Ni(6)-O(55)#1	98.64(14)
O(78)-Ni(7)-O(61)	84.34(16)	O(74)-Ni(6)-O(55)#1	97.29(18)
O(60)-Ni(7)-O(61)	80.24(13)	O(20)-Ni(6)-O(55)#1	155.35(15)
O(28)-Ni(7)-O(61)	92.75(14)	O(48)-Ni(6)-O(55)#1	78.76(14)
O(34)-Ni(7)-O(32)	91.88(14)	O(3)#1-Ni(6)-O(54)	92.04(14)
O(78)-Ni(7)-O(32)	173.49(18)	O(74)-Ni(6)-O(54)	178.36(19)
O(60)-Ni(7)-O(32)	83.41(15)	O(20)-Ni(6)-O(54)	73.03(14)
O(28)-Ni(7)-O(32)	72.83(14)	O(48)-Ni(6)-O(54)	95.04(14)
O(61)-Ni(7)-O(32)	95.88(14)	O(55)#1-Ni(6)-O(54)	84.28(15)
O(20)-Ni(5)-O(26)#1	95.13(14)	O(9)-Ni(4)-O(70)	85.13(16)
O(20)-Ni(5)-O(16)	152.26(14)	O(9)-Ni(4)-O(61)	167.67(15)
O(26)#1-Ni(5)-O(16)	96.34(13)	O(70)-Ni(4)-O(61)	85.72(16)
O(20)-Ni(5)-O(30)	92.25(14)	O(9)-Ni(4)-O(60)	93.68(13)
O(26)#1-Ni(5)-O(30)	90.68(14)	O(70)-Ni(4)-O(60)	98.03(18)
O(16)-Ni(5)-O(30)	112.75(15)	O(61)-Ni(4)-O(60)	79.44(13)
O(20)-Ni(5)-O(46)	93.56(14)	O(9)-Ni(4)-O(11)	88.83(13)
O(26)#1-Ni(5)-O(46)	169.37(14)	O(70)-Ni(4)-O(11)	168.30(17)
O(16)-Ni(5)-O(46)	78.55(13)	O(61)-Ni(4)-O(11)	101.58(13)
O(30)-Ni(5)-O(46)	82.86(14)	O(60)-Ni(4)-O(11)	92.34(14)
O(20)-Ni(5)-O(54)	71.76(13)	O(9)-Ni(4)-O(51)	102.20(13)
O(26)#1-Ni(5)-O(54)	96.64(13)	O(70)-Ni(4)-O(51)	97.16(18)

O(16)-Ni(5)-O(54)	81.87(14)	O(61)-Ni(4)-O(51)	87.13(13)
O(30)-Ni(5)-O(54)	162.89(15)	O(60)-Ni(4)-O(51)	158.85(14)
O(46)-Ni(5)-O(54)	91.88(13)	O(11)-Ni(4)-O(51)	74.31(13)
O(81)#1-Ni(10)-	180.000(1)	O(12)-Ni(3)-O(46)	166.12(15)
O(81)			
O(81)#1-Ni(10)-	81.0(4)	O(12)-Ni(3)-O(16)	95.20(14)
O(79)#1			
O(81)-Ni(10)-	99.0(4)	O(46)-Ni(3)-O(16)	78.89(13)
O(79)#1			
O(81)#1-Ni(10)-	99.0(4)	O(12)-Ni(3)-O(56)	85.06(16)
O(79)			
O(81)-Ni(10)-O(79)	81.0(4)	O(46)-Ni(3)-O(56)	82.92(15)
O(79)#1-Ni(10)-	180.0(2)	O(16)-Ni(3)-O(56)	94.45(17)
O(79)			
O(81)#1-Ni(10)-	89.6(4)	O(12)-Ni(3)-O(42)	101.62(14)
O(80)#1			
O(81)-Ni(10)-	90.4(4)	O(46)-Ni(3)-O(42)	87.81(14)
O(80)#1			
O(79)#1-Ni(10)-	94.5(2)	O(16)-Ni(3)-O(42)	156.85(14)
O(80)#1			
O(79)-Ni(10)-	85.5(2)	O(56)-Ni(3)-O(42)	102.69(16)
O(80)#1			
O(81)#1-Ni(10)-	90.4(4)	O(12)-Ni(3)-O(10)	89.26(13)
O(80)			
O(81)-Ni(10)-O(80)	89.6(4)	O(46)-Ni(3)-O(10)	103.33(13)
O(79)#1-Ni(10)-	85.5(2)	O(16)-Ni(3)-O(10)	91.46(14)
O(80)			
O(79)-Ni(10)-O(80)	94.5(2)	O(56)-Ni(3)-O(10)	172.14(16)
O(80)#1-Ni(10)-	180.000(1)	O(42)-Ni(3)-O(10)	73.13(13)
O(80)			
O(33)-Ni(2)-O(71)	86.78(16)	O(7)-Ni(1)-O(24)	98.59(14)
O(33)-Ni(2)-O(48)	167.79(15)	O(7)-Ni(1)-O(73)	87.78(17)
O(71)-Ni(2)-O(48)	84.52(16)	O(24)-Ni(1)-O(73)	103.7(2)
O(33)-Ni(2)-O(55)#1	94.08(14)	O(7)-Ni(1)-O(28)	95.80(14)
O(71)-Ni(2)-O(55)#1	98.8(2)	O(24)-Ni(1)-O(28)	151.25(14)
O(48)-Ni(2)-O(55)#1	78.85(14)	O(73)-Ni(1)-O(28)	101.56(19)
O(33)-Ni(2)-O(42)	101.87(14)	O(7)-Ni(1)-O(44)	170.19(15)
O(71)-Ni(2)-O(42)	96.85(18)	O(24)-Ni(1)-O(44)	79.62(14)
O(48)-Ni(2)-O(42)	87.68(14)	O(73)-Ni(1)-O(44)	83.32(17)
O(55)#1-Ni(2)-O(42)	158.21(15)	O(28)-Ni(1)-O(44)	90.04(14)
O(33)-Ni(2)-O(10)	86.79(13)	O(7)-Ni(1)-O(32)	97.54(13)
O(71)-Ni(2)-O(10)	166.79(18)	O(24)-Ni(1)-O(32)	83.38(14)
O(48)-Ni(2)-O(10)	103.39(14)	O(73)-Ni(1)-O(32)	170.44(18)
O(55)#1-Ni(2)-O(10)	93.16(14)	O(28)-Ni(1)-O(32)	70.10(13)

O(42)-Ni(2)-O(10)	73.24(13)	O(44)-Ni(1)-O(32)	91.85(13)
-------------------	-----------	-------------------	-----------

Table S3. Comparison haloperoxidase mimic activity of **Ni₁₆Mo₁₆P₂₄** with other materials

	Catalysts	K _m (Br ⁻)	K _m (H ₂ O ₂)	Reference
1	Co-MoS ₂	28 mM	117 μM	S1
2	CeO _{2-x} (R=1)	206.9 mM	476.8 μM	S2
3	Cr-SA-CN	18.1 mM	22 μM	S3
4	Mo SA-N/C	9.9 mM	219.3 μM	S4
5	W-Uio	\	555 μM	S5

6	CeO ₂ @ZrO ₂	22 mM	102 μM	S6
7	CeO ₂ @C	500 mM	2100 μM	S7
8	Ni₁₆Mo₁₆P₂₄	27.72 μM	114.38 μM	This work

Table S4. Comparison H₂O₂ production ability of **Ni₁₆Mo₁₆P₂₄** with other materials

Catalysts	E (vs. RHE)	Production rate (mol·g ⁻¹ ·h ⁻¹)	Reference
CeO ₂ NCs	0.5	0.63	S8
O-P/N-C900	0.1	0.69	S9
rGO/PEI	0.74	0.11	S10
Oxo-G/NH ₃	0.2	0.25	S11
Fe ₂ O _{3-x}	0.1	0.45	S12

NCMK3IL50	0.1	0.56	S13
NOC-6M	0.55	0.55	S14
HNCS	0.4	0.62	S15
Ni₁₆Mo₁₆P₂₄	0.1	0.78	This work

Table S5 Comparison nanozyme performance of **Ni₁₆Mo₁₆P₂₄** with other POMs

	POMs	Activity	Application	Reference
1	GdP ₅ W ₃₀ O ₁₁₀ @WS ₂ NCs	Peroxidase-mimic	H ₂ O ₂ detection	S16
2	n-[Bu ₄ -N] ₂ [Mo ₆ O ₁₈ NC ₁₃ H ₉]	Peroxidase-mimic	H ₂ O ₂ detection	S17

3	GOx-PTA@MS	Peroxidase-mimic	Glucose detection	S18
4	Au@POM NPs	Peroxidase-mimic	bacterial detections	S19
5	CuO NP-POM	Peroxidase-mimic	AA and Fe ²⁺ detection	S20
6	[Ag ₂ (bit) ₂] ₂ [Mo ₈ O ₂₆]	Peroxidase-mimic	L-Cys detection	S21
7	Ni₁₆Mo₁₆P₂₄	Haloperoxidase mimic	antibiofouling	This work

References

- (S1) Q, Luo.; J, Li.; W, Wang.; Y, Li.; Y, Li.; X, Huo.; J, Li.; N, Wang., Transition metal engineering of molybdenum disulfide nanozyme for biomimicking anti-biofouling in seawater. *ACS Appl Mater Interfaces* **2022**, *14*, 14218-14225
- (S2) J, Lang.; X, Ma.; P, Chen.; M. D. Serota; N. M. Andre; G. R. Whittaker; R, Yang., Haloperoxidase-mimicking CeO_{2-x} nanorods for the deactivation of human coronavirus OC43. *Nanoscale* **2022**, *14*, 3731-3737

- (S3) Q, Luo.; Y, Li.; X, Huo.; L, Li.; Y, Song.; S, Chen.; H, Lin.; N, Wang., Atomic chromium coordinated graphitic carbon nitride for bioinspired antibiofouling in seawater. *Adv Sci (Weinh)* **2022**, 9, e2105346
- (S4) W, Wang.; Q, Luo.; J, Li.; L, Li.; Y, Li.; X, Huo.; X, Du.; Z, Li.; N, Wang., Photothermal-amplified single atom nanozyme for biofouling control in seawater. *Adv. Funct. Mater* **2022**, 32, 2205461
- (S5) W, Wang.; Q, Luo.; J, Li.; Y, Li.; R, Wu.; Y, Li.; X, Huo.; N, Wang., Single-atom tungsten engineering of MOFs with biomimetic antibiofilm activity toward robust uranium extraction from seawater. *Chem. Eng. J* **2022**, 431, 133483
- (S6) Q, Luo.; Y, Li.; X, Huo.; J, Li.; L, Li.; W, Wang.; Y, Li.; S, Chen.; Y, Song., N, Wang., Stabilizing ultrasmall ceria-cluster nanozyme for antibacterial and antibiofouling applications. *Small* **2022**, 18, e2107401
- (S7) N, Wang.; W, Li.; Y, Ren.; J, Duan.; X, Zhai.; F, Guan.; L, Wang.; B, Hou., Investigating the properties of nano core-shell CeO₂@C as haloperoxidase mimicry catalyst for antifouling applications. *Colloid Surface A* **2021**, 608, 125592
- (S8) M, Cheng.; Z, Li.; T, Xu.; Y, Mao.; Y, Zhang.; G, Zhang.; Z, Yan, Efficient overall 2e⁻ oxygen electrolysis to H₂O₂ on CeO₂ nanocubes. *Electrochim. Acta* **2022**, 430, 141091
- (S9) Z, Li.; A, Kumar.; N, Liu.; M, Cheng.; C, Zhao.; X, Meng.; H, Li.; Y, Zhang.; Z, Liu.; G, Zhang.; X, Sun., Oxygenated P/N co-doped carbon for efficient 2e⁻ oxygen reduction to H₂O₂. *J. Mater. Chem. A* **2022**, 10, 14355-14363
- (S10) X, Xiao.; T, Wang.; J, Bai.; F, Li.; T, Ma.; Y, Chen., Enhancing the selectivity of H₂O₂ electrogeneration by steric hindrance effect. *ACS Appl. Mater. Interfaces* **2018**, 10, 42534-42541
- (S11) L, Han.; Y, Sun.; S, Li.; C, Cheng.; C, Halbig.; P, Feicht.; J, Hübner.; P, Strasser.; S, Eigler. In-plane carbon lattice-defect regulating electrochemical oxygen reduction to hydrogen peroxide production over nitrogen-doped graphene. *ACS Catal.* **2019**, 9, 1283-1288
- (S12) R, Gao.; L, Pan.; Z, Li.; C, Shi.; Y, Yao.; X, Zhang.; J, Zou. Engineering facets and oxygen vacancies over hematite single crystal for intensified electrocatalytic H₂O₂ production. *Adv. Funct. Mater.* **2020**, 30, 1910539
- (S13) Y, Sun.; I, Sinev.; W, Ju.; A, Bergmann.; S, Dresp.; S, Kühl.; C, Spöri.; H, Schmies.; H, Wang.; D, Bernsmeier.; B, Paul.; R, Schmack.; R, Krahnert.; B, Roldan Cuenya.; P,

Strasser. Efficient electrochemical hydrogen peroxide production from molecular oxygen on nitrogen-doped mesoporous carbon catalysts. *ACS Catal.* **2018**, *8*, 2844-2856

(S14) C, Zhang.; G, Liu.; B, Ning.; S, Qian.; D, Zheng.; L, Wang. Highly efficient electrochemical generation of H₂O₂ on N/O co-modified defective carbon. *Int. J. Hydrogen Energy* **2021**, *46*, 14277-14287

(S15) Y, Hu.; J, Zhang.; T, Shen.; Z, Li.; K, Chen.; Y, Lu.; J, Zhang.; D, Wang. Efficient electrochemical production of H₂O₂ on hollow N-doped carbon nanospheres with abundant micropores. *ACS Appl. Mater. Interfaces* **2021**, *13*, 29551-29557

(S16) G, Du.; M, Lv.; H, Wang.; C, Liu.; Q, Xu.; J, Liu.; Z, Yang.; Y, Yong.; Y, Han., A polyoxometalate-based heterojunction nanozyme with peroxidase-mimic catalytic activity for sensitive biomolecule detection. *Nanoscale Adv* **2023**, *5*, 3985-3993

(S17) M. L. Mujica; I. Sotomayor-Santander; P. Hermosilla-Ibáñez; F. Oyarzun-Ampuero; M. C. Rodríguez; G. A. Rivas; D. Venegas-Yazigi; S. Bollo, MWCNT-organoimido polyoxomolybdate hybrid material: analytical applications for amperometric sensing of hydrogen peroxide. *Electronanal* **2021**, *33*, 2105-2114

(S18) J. Nayak; R. Chilivery; A. K. Kumar; G. Begum; R. K. Rana, A bioinspired assembly to simultaneously heterogenize polyoxometalates as nanozymes and encapsulate enzymes in a microstructure endowing efficient peroxidase-mimicking activity. *ACS sustain Chem Eng.* **2021**, *9*, 15819-15829

(S19) X, Liao.; W, Tong.; L, Dai.; L, Han.; H, Sun.; W, Liu.; C, Wang., Nanozyme-catalyzed cascade reaction enables a highly sensitive detection of live bacteria. *J Mater Chem B* **2023**, *11*, 4890-4898

(S20) Y, Xu.; P, Li.; X, Hu.; H, Chen.; Y, Tang.; Y, Zhu.; X, Zhu.; Y, Zhang.; M, Liu.; S, Yao., Polyoxometalate nanostructures decorated with CuO nanoparticles for sensing ascorbic acid and Fe²⁺ions. *ACS Appl. Nano Mater.* **2021**, *4*, 8302-8313

(S21) B, Li.; H, Chang.; W, Wang.; S, Wang., Study on polyoxomolybdate [Mo₈O₂₆]⁴⁻-based crystalline compound and its polypyrrole nanocomposite as l-cysteine colorimetric biosensor. *J. Clust Sci* **2022**, *33*, 2463–2473

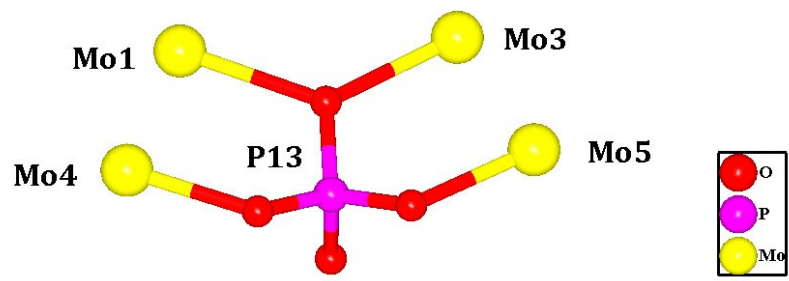


Fig. S1. The coordination mode of PO_4^{3-} group (P13).

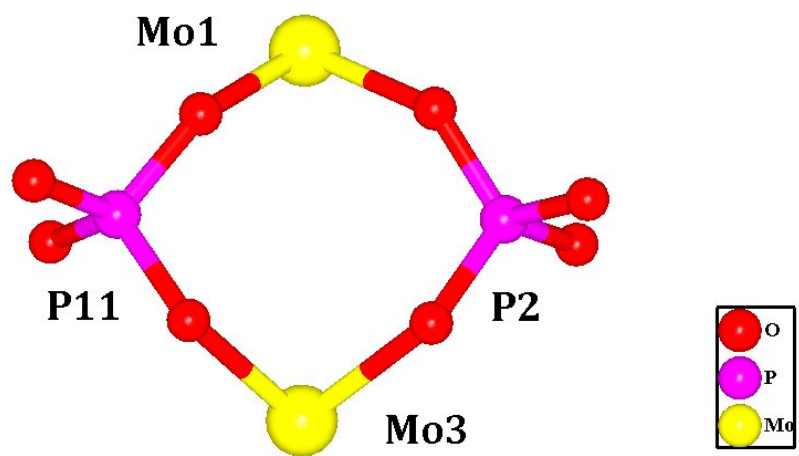


Fig. S2. The coordination modes of two PO_4^{3-} groups (P2 and P11).

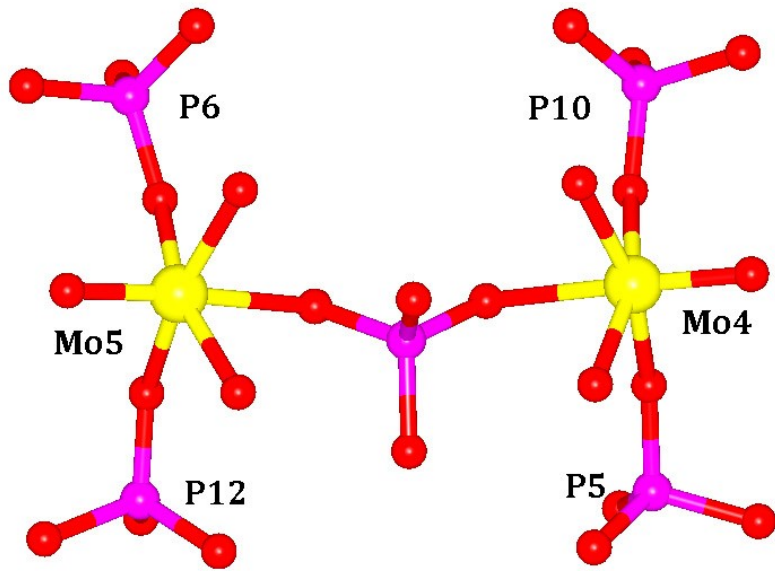


Fig. S3. The coordination modes of four PO_4^{3-} groups (P5, P10 and P6, P12).

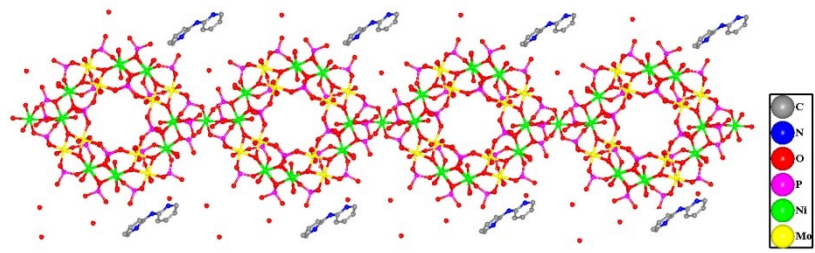


Fig. S4. One-dimensional chain-like structure of $\text{Ni}_{16}\text{Mo}_{16}\text{P}_{24}$.

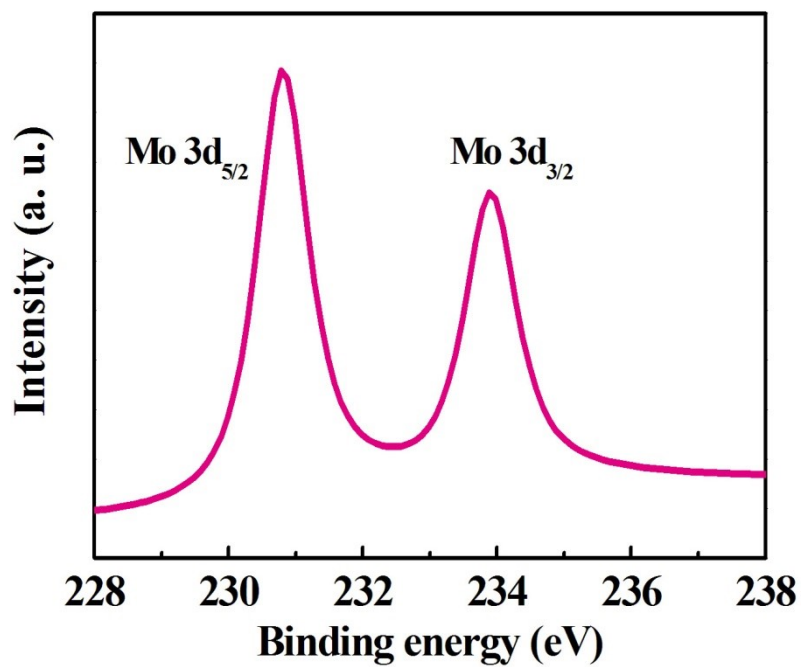


Fig. S5. High resolution Mo 3d XPS spectrum of $\text{Ni}_{16}\text{Mo}_{16}\text{P}_{24}$.

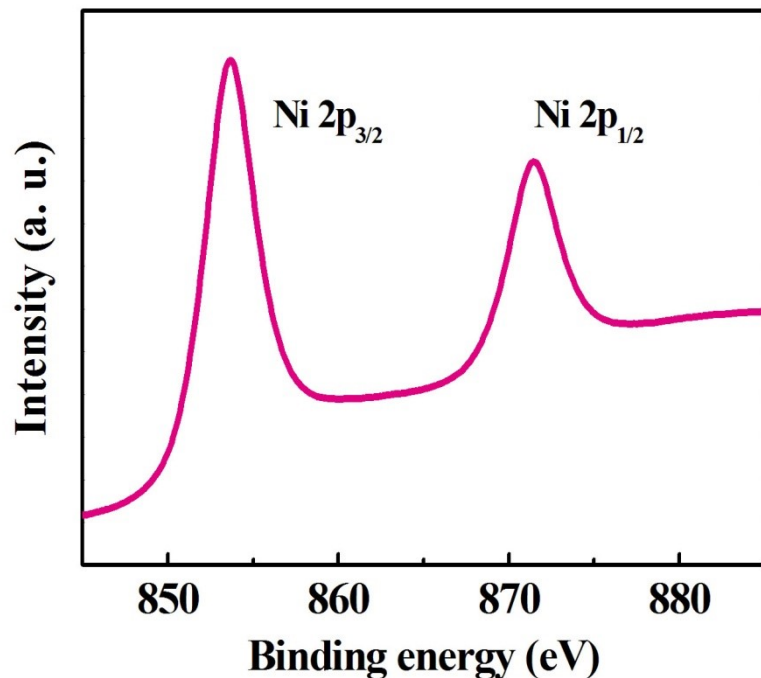


Fig. S6. High resolution Ni 2p XPS spectrum of $\text{Ni}_{16}\text{Mo}_{16}\text{P}_{24}$.

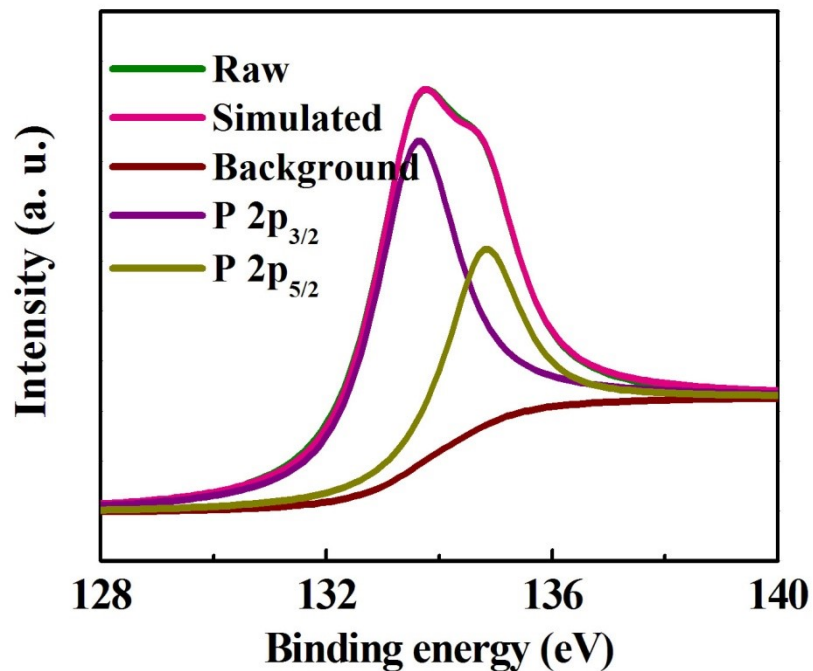


Fig. S7. High resolution P 2p XPS spectrum of $\text{Ni}_{16}\text{Mo}_{16}\text{P}_{24}$.

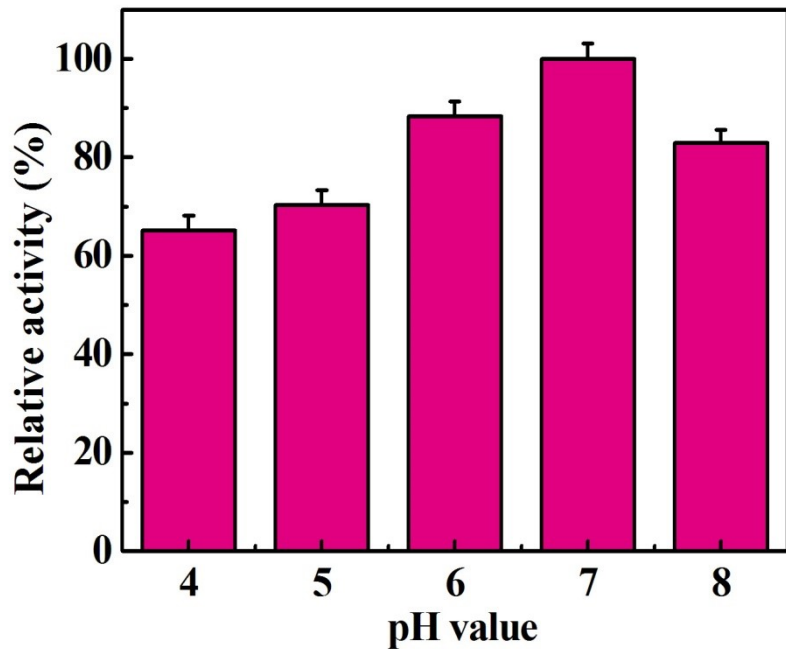


Fig. S8. The influence of pH value on haloperoxidase mimic activity.

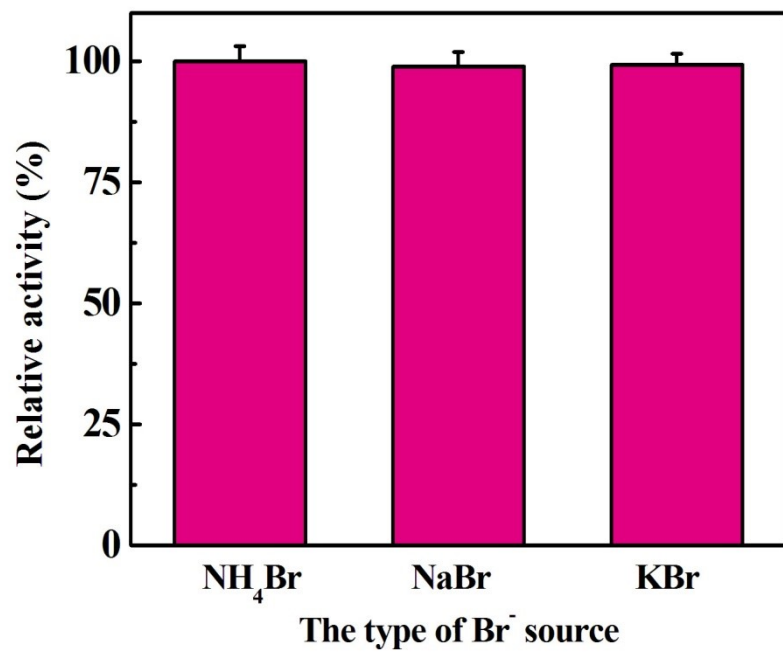


Fig. S9. The influence of temperature on haloperoxidase mimic activity.

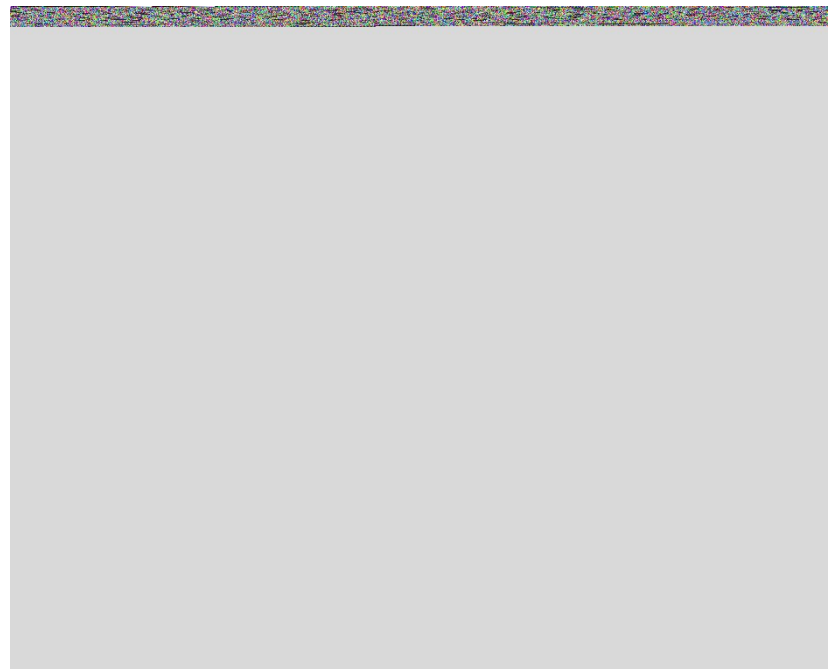


Fig. S10. The influence of Br⁻ resource on haloperoxidase mimic activity.

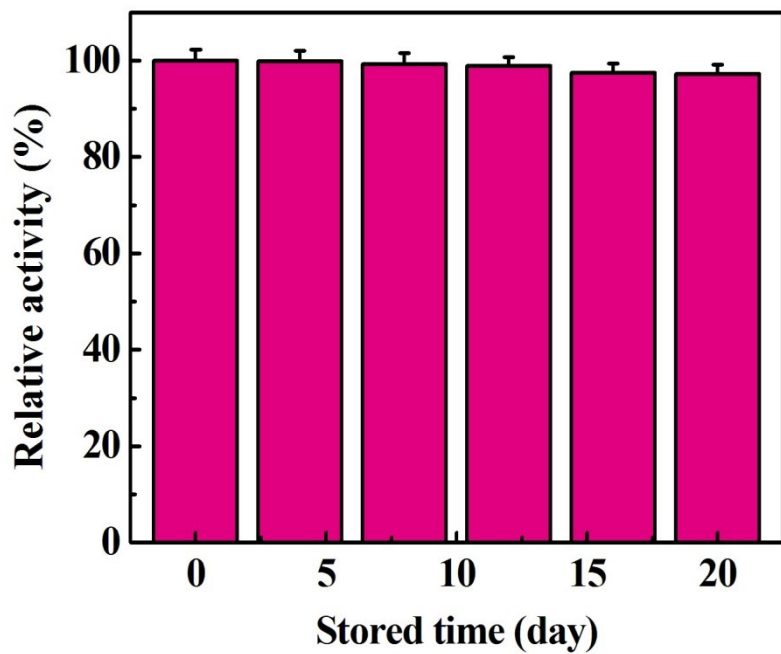


Fig. S11. The influence of stored time on haloperoxidase mimic activity.

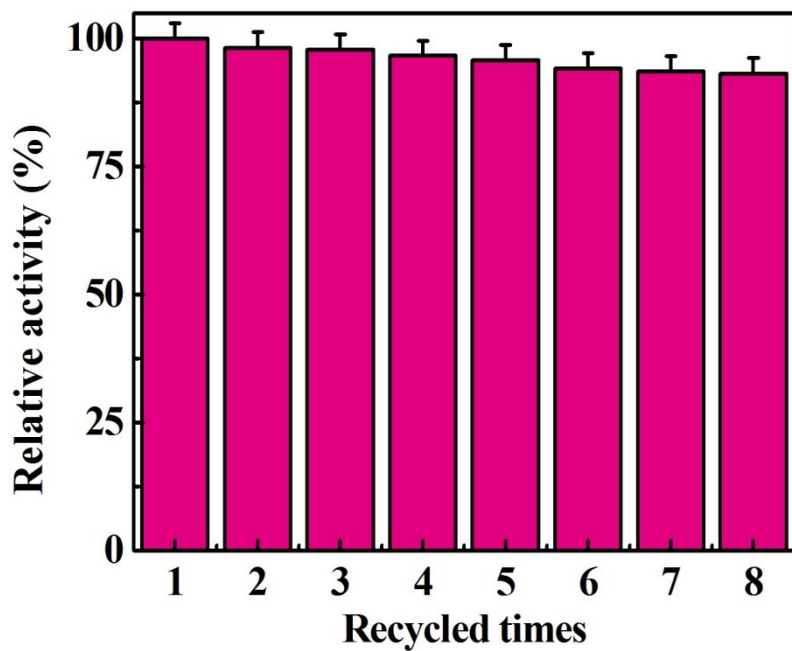


Fig. S12. The influence of recycled times on haloperoxidase mimic activity.

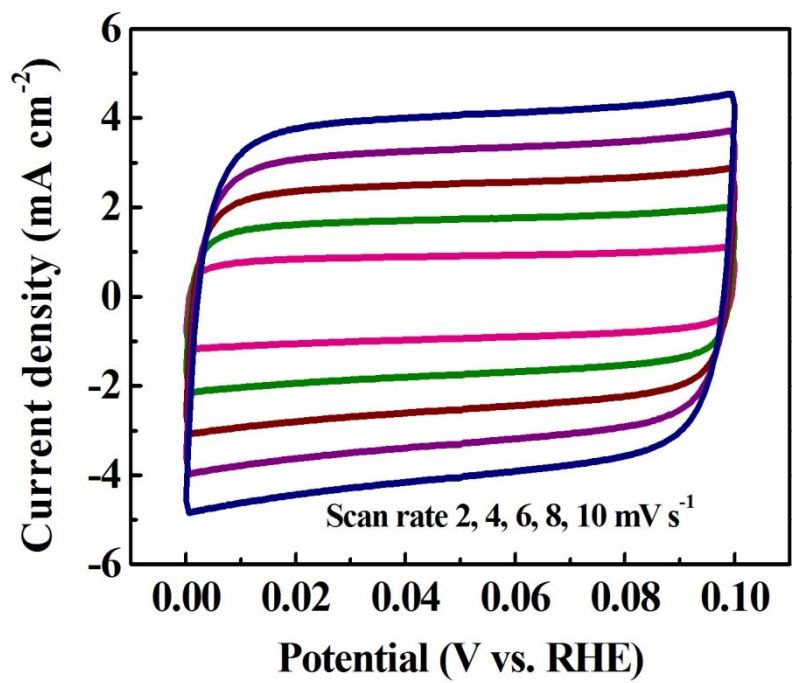


Fig. S13. The CV curves of $\text{Ni}_{16}\text{Mo}_{16}\text{P}_{24}$ at different scanning rates.

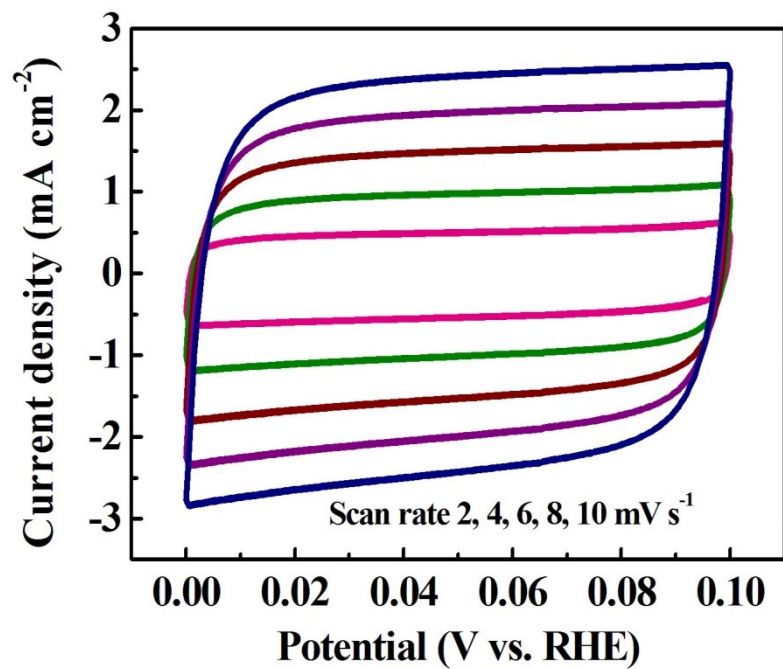


Fig. S14. The CV curves of $\text{Co}_{16}\text{Mo}_{16}\text{P}_{24}$ at different scanning rates.